Article

Joint Sensing and Communications in Unmanned-Aerial-Vehicle-Assisted Systems [†]

Petros S. Bithas [1],[*] , George P. Efthymoglou [2] , Athanasios G. Kanatas [2] and Konstantinos Maliatsos [3]

[1] Digital Industry Technologies, National and Kapodistrian University of Athens, 34400 Psahna, Greece

[2] Digital Systems, University of Piraeus, 18534 Piraeus, Greece; gefthymo@unipi.gr (G.P.E.); kanatas@unipi.gr (A.G.K.)

[3] Information and Communication Systems Engineering, University of the Aegean, 83200 Samos, Greece; kmaliat@aegean.gr

[*] Correspondence: pbithas@dind.uoa.gr

[†] This paper is an extended version of our published paper: Bithas, P.S.; Efthymoglou, G.P.; Kanatas, A.G.; Maliatsos, K. UAV Selection in Aerial Integrated Sensing and Communication Networks. In Proceedings of the IEEE 100th Vehicular Technology Conference (VTCFall), Washington DC, USA, 7–10 October 2024.

Abstract: The application of joint sensing and communications (JSACs) technology in air–ground networks, which include unmanned aerial vehicles (UAVs), offers unique opportunities for improving both sensing and communication performances. However, this type of network is also sensitive to the peculiar characteristics of the aerial communications environment, which include shadowing and scattering caused by man-made structures. This paper investigates an aerial JSAC network and proposes a UAV-selection strategy that is shown to improve the communication performance. We first derive analytical expressions for the received signal-to-interference ratio for both communication and sensing functions. These expressions are then used to analyze the outage and coverage probability of the communication part, as well as the ergodic radar estimation information rate and the detection probability of the sensing part. Moreover, a performance trade-off is investigated under the assumption of a total bandwidth constraint. Various numerical evaluated results have been presented complemented by equivalent simulated ones. These results reveal the applicability of the proposed analysis, as well as the impact of shadowing and multipath fading severity, and interference on the system's performance.

Keywords: bandwidth budget; joint sensing and communications; shadowing; unmanned aerial vehicles (UAVs)

1. Introduction

Joint sensing and communication (JSAC) technology has been proposed as an efficient solution that allows wireless communication and radar sensing coexistence in the same system. The research for JSAC technology has recently gained an increased interest in an effort to effectively exploit the same radio and hardware resources for both sensing and communication functions [1,2]. However, the competition for resources (such as limited power, spectrum, antennas, or other hardware components) between the sensing and communication functions presents a significant challenge that needs to be addressed. It is crucial to identify the key performance boundaries and trade-offs between these functions in JSAC systems subject to resource competition.

In the last few years, various contributions exist that investigate the performance of JSAC systems, e.g., [3–6]. In [3], an integrated sensing and communication (ISAC) system was proposed in which a micro base station (BS) that can simultaneously conduct target sensing and cooperative communication is assumed under a non-orthogonal downlink transmission scenario. In this context, various performance metrics such as outage probability (OP), communication rate, and sensing detection probability (DP) were analyzed.

In [4], a comparison between sensing-communication coexistence (SCC) and JSAC designs utilizing non-orthogonal downlink transmission and transmit antenna selection was performed. Under the assumption of residual hardware impairments and imperfect successive interference cancellation, the performance of the schemes under consideration was evaluated based on the criteria of exact and asymptotic OPs and the probability of successful target detection. In [5], the performance trade-off within the distributed ISAC networks was analytically evaluated based on the tools of stochastic analysis and stochastic geometry. Through these analytical findings, a detailed presentation of the performance boundaries and trade-offs between sensing and communication within a distributed ISAC network was given. In [6], a collaborative ISAC network was investigated that exploits coordinated beamforming techniques. In this framework, the signal-to-interference ratio (SIR) statistics were investigated in order to evaluate the spectral efficiency of the proposed scheme.

Unmanned aerial vehicles (UAVs) have been adopted as an efficient approach for improving coverage probability in various application scenarios, especially when fast deployment is required [7]. Undoubtedly, their benefits are the main reason why UAVs have also been adopted in JSAC scenarios in order to exploit the synergy between these two technologies for a more efficient use of onboard resources, resulting in improved overall performance [8]. To this aim, recently, a numerous of contributions have been presented that investigate JSAC in UAV-assisted communication scenarios, e.g., [9–12]. In [9], a collaborative JSAC and UAV-assisted network is proposed, in which beam sharing opportunities are adopted. In this context, a novel upper-bound average cooperative sensing area performance metric is also proposed, which illustrated the performance improvement of the investigated strategy. In [10], a cellular UAV-assisted network is considered in which communication function is performed jointly with sensing. In this context, the collision probability is analytically investigated, taking into account the radar cross section (RCS) characteristics. In [11], an air–ground JSAC network was examined, which involves unmanned aerial vehicles (UAVs) and ground terrestrial networks. For this important communication scenario, the system architecture and protocol design were explored for four potential use cases, followed by an analysis of the air–ground JSAC (AG-JSAC) network characteristics and advantages. In [12], the network layer delay violation is analyzed in an ISAC and UAV-assisted communication scenario. Among other investigations, the successful sensing probability was analytically studied. A common characteristic of the previously presented results is that the shadowing effects have not been taken into account, despite the fact that in aerial communication networks, the effect of large scale fading is dominant.

Motivated by this observation, in this paper, we consider an aerial-JSAC communication network operating over a generic channel model in which the impact of large scale fading is also taken into account. In this type of network, the radio signals transmitted by a UAV-BS, after having traveled through free space, encounter an urban environment and arrive at the destination. In this urban setting, the signals experience shadowing and scattering due to man-made structures, resulting in extra loss for the air-to-ground link. Based on this system model, our contributions can be summarized as follows:

- We consider a new low-complexity UAV-selection strategy that offers improved performance with reduced complexity, as compared to benchmarks.
- For this scheme, we derive new exact expressions for the statistics of the received SIR, which are then used to investigate various communication and sensing performance metrics, such as the OP, the coverage probability (CP), the DP, and the ergodic radar estimation information rate (EREIR).
- Moreover, the DP and CP performance trade-off is also investigated, having as a parameter of interest the bandwidth that is used for sensing and communication.
- The numerical results presented depict the impact of the shadowing parameter values and the number of interfering signals on the system's performance.

The main objective of this study is to investigate the impact of shadowing in the performance of JSAC networks.

The remainder of this paper is organized as follows. In Section 2, the system model of the JSAC aerial network and the corresponding channel model are provided. In Section 3, the analytical framework for obtaining the performance measures for both JSAC functions is presented. In Section 4, the simulation settings are given, and based on them, various numerical evaluated results are discussed. Finally, this paper's conclusions are drawn in Section 5.

2. System and Channel Models

We consider a JSAC UAV-assisted communication network in which one out of L UAVs, which operate as aerial BSs, is selected to communicate with the destination receiver, as depicted in Figure 1. Moreover, UAVs are also responsible for sensing the surrounding environment in order to identify specific targets. Here, the investigation focuses on the downlink for the communication function. However, exploiting the channel reciprocity principle, similar results are expected to be observed for the uplink performance. A bandwidth division principle between sensing and communication functions is assumed, similar to [13]. According to this, the available bandwidth is split into two portions, bandwidth only for communication purposes and bandwidth only for sensing. It is noted that the basic outcomes of the paper are also valid for the scenario in which the time division approach is employed, since the same interfering effects are expected to be present. During the sensing phase, each of the available UAVs, which are equipped with an active, monostatic, pulsed radar, exploits the intervals of pulses to detect the radar targets. On the other hand, at the communication phase, a selected UAV communicates with the target receiver. However, in both the destination and the UAV radars, interfering signals are also received due to transmissions and echoes from surrounding UAVs. In any case, all channels considered in this study are assumed to be independent.
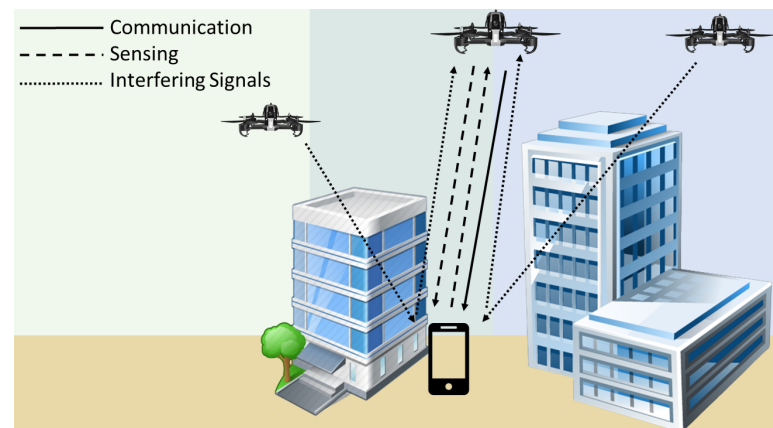
Figure 1. System model of the considered JSAC scheme.

2.1. Channel Model

For the aerial channel model both the effects of small scale fading and large scale fading (shadowing) are taken into account. More specifically, Nakagami-m distribution is considered, which has been found to provide an excellent fit to the fading conditions observed in UAV-to-ground scenarios [14]. The probability density function (PDF) of the random variable g, which models the Nakagami-m distributed channel gain, is given by ([15] [eq. (2.20)]).

$$f_g(x) = \frac{m^m x^{m-1}}{\Omega^m \Gamma(m)} \exp\left(-\frac{mx}{\Omega}\right),\tag{1}$$

where m is distribution's shaping parameter, related to the severity of the fading, Ω denotes the mean square value, and $\Gamma(\cdot)$ is the gamma function ([16] [eq. (8.310/1)]). The corresponding CDF expression is given by

$$F_g(x) = \frac{\gamma(m, \frac{mx}{\Omega})}{\Gamma(m)},$$ (2)

where $\gamma(\cdot, \cdot)$ denotes the lower incomplete gamma function ([16] [eq. (8.350/1)]). It is noted that this type of shadowing modeling is directly related to the probability of obtaining line-of-sight propagation conditions between the two ends of communication [17].

As far as the shadowing effects are concerned, they appear due to the presence of large scale obstacles between the UAVs and the receiver. These shadowing random fluctuations are modeled by the inverse gamma (IG) distribution with PDF given by [14]

$$f_{s_j}(y) = \frac{\overline{\gamma}_j^{\alpha_j}}{\Gamma(\alpha_j)y^{\alpha_j+1}} \exp\left(-\frac{\overline{\gamma}_j}{y}\right),$$ (3)

where $\alpha_j > 1$ is the shaping parameter of the distribution, related to the severity of the shadowing, i.e., lower values of α_j result in lighter shadowing conditions, and $\overline{\gamma}_j$ denotes the scaling parameter. Moreover, the CDF of s_j is given by

$$F_{s_j}(y) = \frac{\Gamma(\alpha_j, \frac{\overline{\gamma}_j}{y})}{\Gamma(\alpha_j)},$$ (4)

where $\Gamma(\cdot, \cdot)$ denotes the upper incomplete gamma function ([16] [eq. (8.350/2)]).

As far as the sensing function is concerned, using advanced signal processing techniques, for analyzing the time delay, amplitude, phase of the reflected signals, and avoiding synchronization error, the received echo signal at a UAV is given by [18]

$$P_{ech} = \frac{p_s G_t G_r \lambda^2 \sigma}{(4\pi)^3 d^{2\nu}},$$ (5)

where p_s denotes the transmitting power of the sensing signal; G_t and G_r denote the transmitting and receiving antenna gains, respectively; λ is the wavelength of the sensing signal; d denotes the distance between the sensing target and the UAV; ν is the path loss factor; and σ is the cross-section of the target. The latter one is a random variable, since it fluctuates from scan to scan, and it follows the Swerling type-1 model, whose PDF is given by [19]

$$f_\sigma(\sigma) = \frac{1}{\bar{\sigma}} \exp\left(-\frac{\sigma}{\bar{\sigma}}\right), \sigma \geq 0,$$ (6)

where $\bar{\sigma}$ is the average cross section over all target fluctuations.

2.2. Communication Model

As far as the communication part is concerned, it is assumed that the UE is connected to the UAV that is less exposed to the shadowing effects. In this approach, which was also adopted in [20], the stationarity region is exploited, based on the fact that the decorrelation distance of the large-scale fading is two orders of magnitude larger than the one of small-scale fading. In this context, the UAV that provides the maximum averaged received power, i.e., shadowing variable, over a predetermined time interval is the one that is selected for communication purposes. After the selection is performed, the selected UAV is informed to proceed with the signal transmission. It is noted that the path loss coefficient can be very easily incorporated in our shadowing-based selection strategy by modifying the scale parameter of the shadowing coefficient. Moreover, assuming that the noise level is relatively small compared to the aggregate interference, we focus on the interference

limited scenario. This type of networks arises in dense cell scenarios, in which severe interference is expected and thus noise can be disregarded, resulting in the SIR being the basis for performance evaluation [21]. Under this UAV-selection policy and based on the approach initially proposed in [20], the received SIR can be expressed as

$$\gamma_c = \frac{p_c G_t G_r g s_{\max} d^{-\nu}}{I_c}, \tag{7}$$

where p_c denotes the transmit power at the communication phase, and $s_{\max} = \max\{s_1, s_2, \cdots, s_L\}$ denotes the maximum shadowing coefficient from the L available UAV-receiver links. Moreover, $I_c = \sum_{i=1}^{M} p_c G_t G_r h_{1,i}^2 d_i^{-\nu}$ denotes the aggregate interference term, with $h_{1,i}$ being the channel gains for the downlink, and d_i is the distance between the i-th, $i = 1, \ldots, M$ interfering UAV and the receiver.

2.3. Sensing Model

During the sensing phase, the detection decisions are conducted by using the target echo power P_{ech}. Based on this approach, the received SIR at the UAV that senses the target is given by [5]

$$\gamma_s = \frac{P_{ech}}{I_s}, \tag{8}$$

where $I_s = \sum_{i=1}^{M} A_e S h_{1,i}^2 h_{2,i}^2 d_i^{-\nu}$ denotes the aggregate interference term; $h_{1,i}$ and $h_{2,i}$, $i = 1, \ldots, M$, denote channel gains that follow Nakagami-m fading; $A_e = \frac{G_r \lambda_w^2}{4\pi}$ denotes the effective receiving antenna aperture; and $S = \frac{p_s G_t}{4\pi}$ denotes the power density from an interfering UAV.

3. Performance Analysis

For the communication part, the performance of the system under investigation is investigated using the criteria of the OP and the CP, while for the sensing part, the performance metrics that are employed are the EREIR and the DP. The CP is defined as the probability that the achievable transmission capacity is above a predefined threshold γ_{th}, i.e.,

$$P_C = P(\gamma_c > 2^{\frac{\gamma_{th}}{B_c}} - 1), \tag{9}$$

where B_c denotes the bandwidth allocated for communication purposes. Based on the CP criterion, the OP is defined as $P_{out} = 1 - P_C$. Moreover, the EREIR is defined as [5]

$$R_B = \frac{\delta}{2T} \log_2(1 + 2TB_s \gamma_s), \tag{10}$$

where T denotes the pulse duration, B_s denotes the bandwidth allocated for sensing purposes, and δ denotes the radar duty cycle. Based on the EREIR, the criterion of DP is defined as follows:

$$P_D = \Pr[R_B > \gamma_{th}] = \Pr\left[\gamma_s > \frac{2^{\frac{2T\gamma_{th}}{\delta}} - 1}{2TB_s}\right], \tag{11}$$

where γ_{th} denotes the detection threshold.

3.1. Communication Function

In this subsection, the analytical framework related to the communication part is presented. For evaluating the performance of the scheme under consideration, the behavior

of the received SIR is statistically evaluated. To this aim, let us define the random variable $Y = \frac{g}{I_c}$. The PDF and CDF of Y are, respectively, given by

$$f_Y(y) = \int_0^\infty x f_g(yx) f_{I_c}(x) dx \tag{12}$$

$$F_Y(y) = \int_0^\infty F_g(yx) f_{I_c}(x) dx. \tag{13}$$

The statistics of I_c are provided in Appendix A. Substituting (1) and (A3) in (12) and using the definition of the gamma function ([16], eq. (8.310)), yields the following analytical expression for the PDF of Y:

$$f_Y(y) = C \sum_{k=0}^\infty \frac{\delta_k}{\Gamma(\rho+k)\beta_1^{\rho+k}} \frac{m^m}{\Omega^m \Gamma(m)} y^{m-1} \left(\frac{1}{\beta_1} + \frac{y}{\Omega} \right)^{-k-m-\rho}. \tag{14}$$

As far as the CDF of Y is concerned, substituting (2) and (A3) in (13), using ([16] [eq. (6.455)]) and after some mathematical manipulations, yields the following expression:

$$F_Y(y) = C \sum_{k=0}^\infty \frac{\delta_k}{\Gamma(\rho+k)\beta_1^{\rho+k}} \left(\frac{y}{\Omega} \right)^m \frac{\Gamma(\rho+k+m)}{m\Gamma(m)}$$
$$\times \,_2F_1 \left(1, \rho+k+m; m+1; \frac{y/\Omega}{y/\Omega + 1/\beta_1} \right) \left(\frac{1}{\beta_1} + \frac{y}{\Omega} \right)^{-k-m-\rho}, \tag{15}$$

where $_2F_1(\cdot)$ denotes the Gauss hypergeometric function ([16] [eq. (9.100)]).

For evaluating the final CDF of γ_c, the statistics of $s_{\max}$ are required, which are provided in Appendix B. Therefore, using (14) and (A8) in (13) results in the following type of integral:

$$\mathcal{I} = \int_0^\infty \left(\frac{y}{x} \right)^{m-1} \left(\frac{1}{\beta_1} + \frac{y}{x\Omega} \right)^{-k-m-\rho} \exp\left(-\frac{\bar\gamma M}{x} \right) \left(\frac{\bar\gamma}{x} \right)^\xi dx, \tag{16}$$

where $\xi = \sum_{i=0}^{\alpha-1} i n_{i+1}$, with n_is denoting integers related to the multiple sums presented below. In order to evaluate this integral, the Meijer G-function representations of the constitute functions are employed, using ([22] [eqs. (10) and (11)]), as follows:

$$\left(\frac{1}{\beta_1} + \frac{y}{x\Omega} \right)^{-k-m-\rho} = \left(\frac{1}{\beta_1} \right)^{-k-m-\rho} \frac{1}{\Gamma(k+m+\rho)} G_{1,1}^{1,1} \left(\frac{\beta_1 y}{x\Omega} \middle| \begin{matrix} 1-k-m-\rho \\ 0 \end{matrix} \right),$$
$$\exp\left(-\frac{\bar\gamma M}{x} \right) = G_{0,1}^{1,0} \left(\frac{\bar\gamma M}{x} \middle| \begin{matrix} - \\ 0 \end{matrix} \right), \tag{17}$$

where $G_{p,q}^{m,n}(\cdot|\cdot)$ denotes the Meijer G-function. Based on these expressions, using ([22] [eq. (21)]), after some analysis, results in

$$F_{\gamma_c}(x) = C \sum_{k=0}^\infty \sum_{\substack{n_1=0 \\ n_1+n_2+\cdots+n_\alpha=M}}^M \sum_{n_2=0}^M \cdots \sum_{n_\alpha=0}^M \left(\frac{\bar\gamma_c}{x} \right)^\xi \frac{M!}{n_1! n_2! \cdots n_\alpha!} \delta_k \Gamma(m+k+\rho) \left[\prod_{i=0}^{\alpha-1} \left(\frac{1}{i!} \right)^{n_{i+1}} \right]$$
$$\times \left[\frac{\Gamma(m+\xi)\Gamma(k-\xi+\rho)}{\Gamma(m+k+\rho)} \left(\frac{\beta_1}{\Omega} \right)^{-m-\xi} \,_1F_1 \left(m+\xi, 1-k+\xi-\rho, \frac{M\bar\gamma_c\Omega}{\beta_1 x} \right) \right. \tag{18}$$
$$\left. - \Gamma(-k+\xi-\rho) \left(\frac{M\bar\gamma_c}{x} \right)^{k-\xi+\rho} \left(\frac{\beta_1}{\Omega} \right)^{-m-k-\rho} \,_1F_1 \left(m+k+\rho, 1+k-\xi+\rho, \frac{M\bar\gamma_c\Omega}{\beta_1 x} \right) \right],$$

where $_1F_1(\cdot)$ denotes the confluent hypergeometric function ([16] [eq. (9.210/1)]), while $\bar{\gamma}_c = \bar{\gamma} p_c G_t G_r d^{-\nu}$.

3.2. Sensing Function

In this subsection, the analytical framework related to the sensing part is presented. For evaluating the sensing performance, the statistical behavior of the corresponding received SIR is evaluated. To this aim, let us define the random variable $W = \frac{\sigma}{I_s}$. For evaluating the PDF of W, a similar procedure to the one used in the derivation of (14) is adopted, resulting in

$$f_W(y) = C \sum_{k=0}^{\infty} \frac{\delta_k}{\bar{\sigma}\Gamma(\rho+k)\beta_1^{\rho+k}} \left(\frac{1}{\beta_1} + \frac{y}{\bar{\sigma}}\right)^{-k-1-\rho}. \tag{19}$$

The corresponding CDF can be derived as

$$F_W(y) = C \sum_{k=0}^{\infty} \frac{\delta_k}{\Gamma(\rho+k+1)} \left(1 - \left(1 + \frac{\beta_1 y}{\bar{\sigma}}\right)^{-k-1-\rho}\right). \tag{20}$$

Based on (19), the PDF of γ_s can be directly evaluated using a change in variables of the form $W = \gamma_s \frac{(4\pi)^3 d^{2\nu}}{p_s G_t G_r \lambda^2}$, which results in a similar expression to (19), where $\bar{\sigma}$ is substituted with $\bar{\gamma}_\sigma = \bar{\sigma} \frac{p_s G_t G_r \lambda^2}{(4\pi)^3 d^{2\nu}}$. For evaluating the expression for the EREIR, (19) should be substituted in (10). Following such an approach, integrals of the following form need to be solved:

$$\mathcal{I}_2 = \int_0^{\infty} \left(\frac{1}{\beta_1} + \frac{x}{\bar{\gamma}_\sigma}\right)^{-k-1-\rho} \log_2(1 + 2TB_s x) dx. \tag{21}$$

Using again the Meijer-G function representations for the functions in (21), i.e., using ([22] [eqs. (10) and (11)]),

$$\ln(1+x) = G_{2,2}^{1,2}\left(x \Big|_{1,0}^{1,1}\right), \tag{22}$$

as well as ([22] [eqs. (21)]), yields the following exact expression

$$R_B = \frac{\delta}{2T} C \sum_{k=0}^{\infty} \frac{\delta_k / \ln(2)}{\Gamma(\rho+k)\Gamma(1+k+\rho)} G_{3,3}^{2,3}\left(\frac{2B_s T \bar{\gamma}_\sigma}{\beta_1} \Big|_{1,k+\rho,0}^{1,1,0}\right). \tag{23}$$

It is noted that with a small number of terms, i.e., < 20, a satisfactory accuracy is observed, i.e., which guarantees accuracy better than $\pm 0.5\%$, in all infinite series expressions derived in this paper.

3.3. Performance Trade-Off

In the system under consideration, the performance trade-off between the sensing and communication functions can be analyzed. One of the key factors that influences this trade-off is to allocate different portions of the frequency spectrum to the sensing and communication functions. In this frequency-division approach, part of the total bandwidth is dedicated to transmitting the sensing waveform, while the remaining portion is used for transmitting the communication signal. This leads to a bandwidth allocation trade-off, which can be expressed as follows: [23]

$$B_s + B_c = B. \tag{24}$$

In the numerical results section, we investigate the performance trade-off between communication and sensing functions when we allocate different portions of the total available bandwidth B to B_c and B_s.

4. Numerical Results

In this section, based on the analytical results derived previously, several numerical evaluated results are presented and discussed. These results have been evaluated using the Matlab 2021$^{®}$ mathematical software package. If not otherwise stated, in the simulation results, the parameter values depicted in Table 1 are assumed, which, in general, model a dense cell scenario where moderate fading and shadowing conditions can be found.

Table 1. Simulation Parameter Values [5].

General Parameters	Values
Wavelength (λ)	0.0833 m
Transmit Power (P_c)	15 dBm
Tx Antenna Gain (G_t)	10 dB
Rx Antenna Gain (G_r)	10 dB
Tx-Rx Distance (d)	80 m
Path Loss Factor (ν)	2
Shadowing Coefficient (α)	2
Number of Interfering Signals (M)	9
Communication Parameters	**Values**
Nakagami Parameter (m) for all links	2
Number of UAVs (L)	4
Bandwidth (B_c)	20 MHz
Sensing Parameters	**Values**
Bandwidth (B_s)	20 MHz
Pulse Duration (T)	1 μs
Radar Duty Cycle (δ)	0.01

In Figure 2, the OP and DP performances have been evaluated. More specifically, in the left subplot, the OP using UAV-selection is plotted as a function of the outage threshold γ_{th} for various values of the shadowing coefficients $\alpha = \alpha_j$, $j = 1, \ldots, L$. It is shown that for the same γ_{th}, almost ten times less OP is observed when light shadowing conditions are assumed, i.e., $\alpha = 1$, compared to moderate shadowing, $\alpha = 3$. In the same figure, for comparison purposes, the performance of a scheme without UAV-selection is also presented. It is shown that the performance of the UAV-selection scheme is considerably improved, especially in the case of severe shadowing conditions. In the right subplot of Figure 2, the EREIR is plotted as a function of the transmit power for different distances of the radar target. The plot shows the performance degradation of the sensing function, evaluated using the EREIR, as the distance increases.

In Figure 3, we investigate the effect of aggregate interference by plotting the CP (with $\gamma_{\text{th}} = 0$ dB) and the DP as a function of the transmit power for different values of the number of interfering signals. It is shown that the number of interfering signals has an important influence on the performance of both functions, which reduces as M increases. One of the main results of this paper is illustrated in Figure 4, in which the fundamental performance trade-off between communication and sensing functions under specific bandwidth constraint, i.e., $B = 20$ MHz, is presented. It is noted that the sum of the bandwidths B_c and B_s is limited by the total available one B, and thus it is impossible to simultaneously obtain optimal performance for both these functions. However, a useful balance can be achieved as is depicted in Figure 4. In this figure, it is shown that by dedicating a large portion to the communication bandwidth B_c, the CP increases, but the DP decreases, since a reduction in B_s is required in order to satisfy the fixed total bandwidth. The results also show that the variations in the bandwidth have a greater impact on the communication performance than on sensing. For example, as B_c reduces from 20 MHz to 0, which results in an increase in B_s from 0 to 20 MHz), the CP drops from 1 to 0, while

DP increases from 0 to 0.2, as shown by the yellow curve. In the same figure, it is also illustrated that as the distance between the UAV and the destination/target d increases, the impact of the modification of the B_s at the DP increases. Here, it should be noted that the optimal interplay between the detection and coverage probabilities could be investigated in an optimization framework, in which the decision variables and constraints could be the bandwidth and the power allocation.
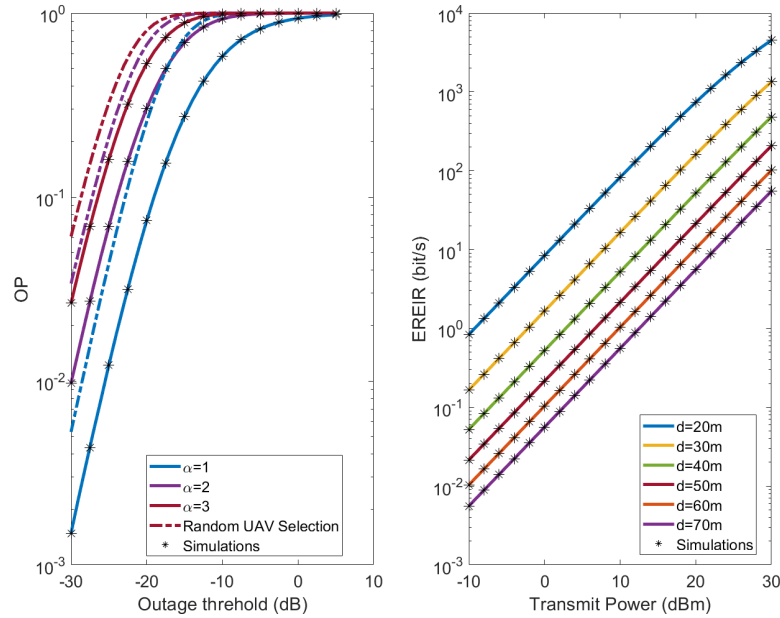

Figure 2. Communication Function: OP vs. the outage threshold. Sensing Function: EREIR vs. transmit power.
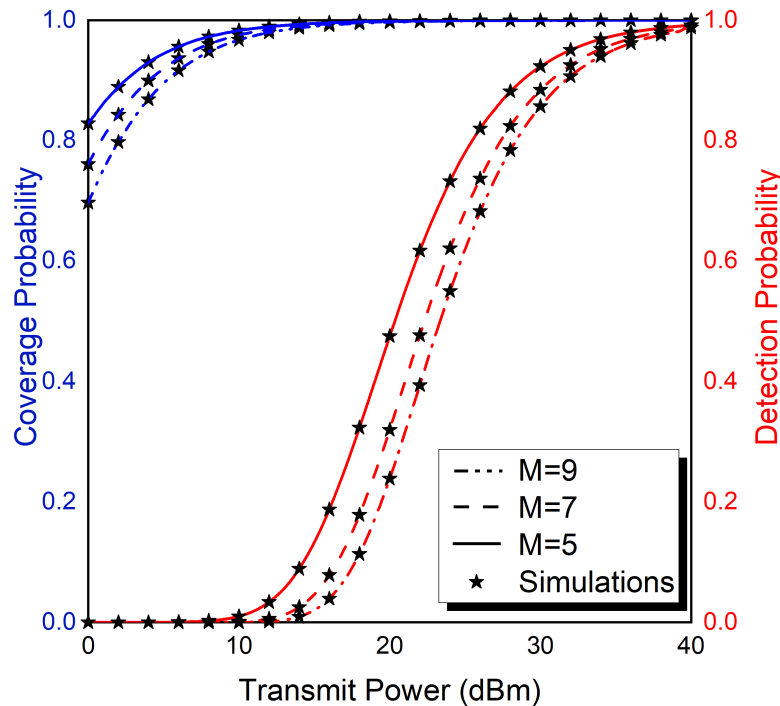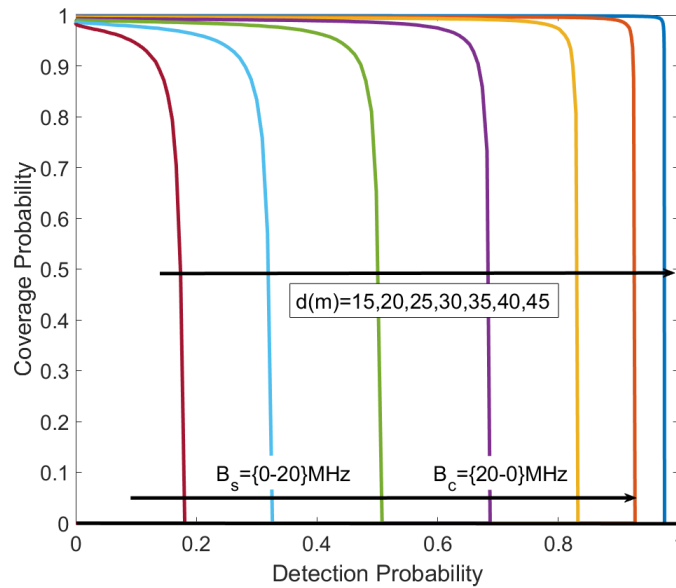

Figure 3. Coverage probability and detection probability vs. transmit power for different number of interfering sources.

Figure 4. Coverage probability and detection probability trade-off under bandwidth allocation for different distances.

In Figure 5, the impact of the multipath fading severity is investigated. In particular, in this figure, the OP is plotted as a function of the threshold for different multipath fading conditions, which are controlled by shaping parameter m. It is shown a performance improvement as the severity of the fading lessens, i.e., m increases. In Figure 6, the impact of the number of UAVs L is investigated. In particular, in this figure, the OP is plotted as a function of the threshold for different values of the number of UAVs. The performance improvement that is achieved as L increases is shown. However, the rate of the improvement lessens for higher values of L. Finally, it is noted that in all figures presented, simulation results have also been included, verifying the validity of the presented analytical framework.
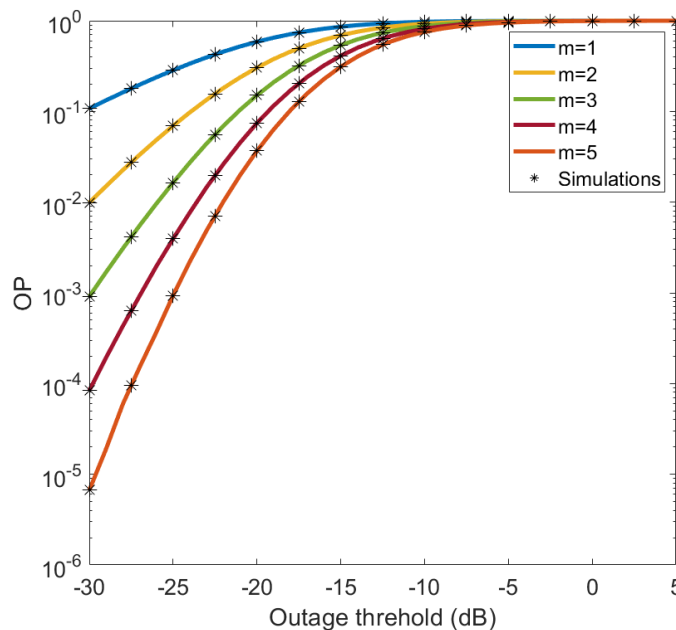
Figure 5. Outage probability vs. the outage threshold for different values of m.
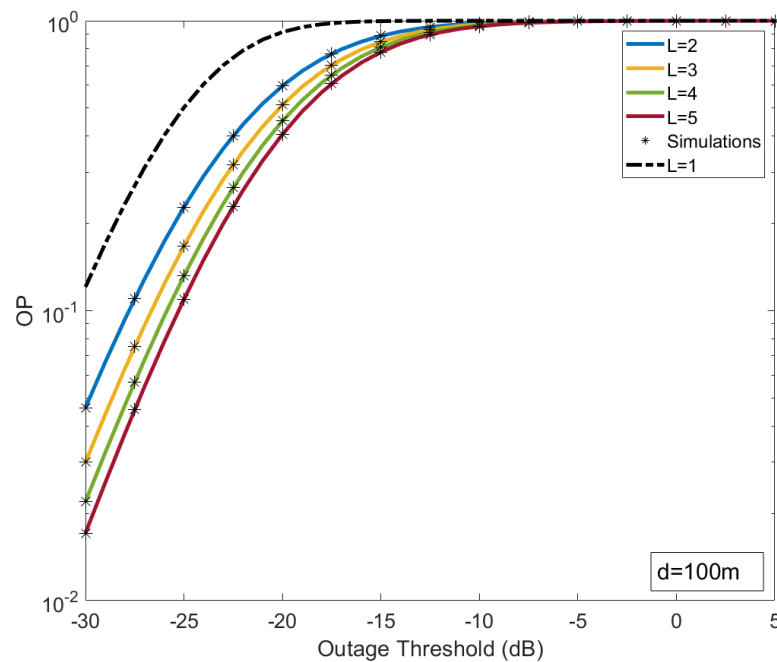
Figure 6. Outage probability vs. the outage threshold for different values of *L*.

5. Conclusions

In this paper, a new UAV-selection strategy is proposed for an aerial JSAC network operating in a composite fading environment. To this aim, we presented an analytical framework used to evaluate the coverage probability of the scheme under consideration and the EREIR of each UAV. The presented results revealed the impact of shadowing and interference on the system's performance. It was shown that a performance trade-off exists in frequency division JSAC scenarios. Moreover, the numerical results presented revealed that the performance of the communication function can be considerably improved using a shadowing-based UAV-selection policy. Our next steps include an analytical investigation in a more general scenario in which the impact of the noise, shadowing correlation, and the antenna patterns will be also taken into account. Finally, an interesting future direction includes an optimization framework for analytically investigating the bandwidth allocation trade-off.

Author Contributions: Conceptualization, P.S.B. and A.G.K.; methodology, P.S.B.; software, P.S.B. and K.M.; investigation, P.S.B. and G.P.E.; writing—original draft preparation, P.S.B.; writing—review and editing, K.M., G.P.E., and A.G.K. All authors have read and agreed to the published version of the manuscript.

Data Availability Statement: The original contributions presented in the study are included in the article, further inquiries can be directed to the corresponding author.

Conflicts of Interest: The authors declare no conflicts of interest.

Abbreviations

The following abbreviations are used in this manuscript:

CDF	Cumulative distribution function
CP	Coverage probability
DP	Detection probability
EREIR	Ergodic radar estimation information rate
ISAC	Integrate sensing and communication
JSAC	Joint sensing and communication

OP   Outage probability
PDF   Probability density function
SIR   Signal-to-interference ratio
SNR   Signal-to-noise ratio
UAV   Unmanned aerial vehicle

Appendix A

In this appendix, a convenient exact expression for the PDF of the aggregate interference terms for the communication function is presented. Let us assume that RV I_i is defined as follows:

$$I_i = p_c G_t G_r h_{1,i}^2 d_i^{-\nu}. \tag{A1}$$

Here, RV I_i is approximated by a gamma RV G_i, whose shaping and scaling parameters can be evaluated using the moment matching method, e.g., [24]. Based on this assumption, I_i is now represented by a sum of M gamma RVs given as follows:

$$I_q = G_1 + G_2 + \cdots + G_M, \tag{A2}$$

where $q \in \{s, c\}$. Based on the results presented in [25], the PDF of I_q can be expressed as follows:

$$f_{I_q}(x) = C \sum_{k=0}^{\infty} \frac{\delta_k x^{\rho+k-1}}{\Gamma(\rho+k)\beta_1^{\rho+k}} \exp\left(-\frac{x}{\beta_1}\right), \tag{A3}$$

where $\beta_i = \frac{\Omega_i}{m_i}$, $\beta_1 = min(\beta_i)$, while

$$C = \prod_{i=1}^{M}\left(\frac{\beta_1}{\beta_i}\right)^{m_i}, \ \rho = \sum_{i=1}^{M} m_i, \ \gamma_k = \sum_{i=1}^{M} \frac{m_i}{k}\left(1 - \frac{\beta_1}{\beta_i}\right)^k \tag{A4}$$

$$\delta_{k+1} = \frac{1}{k+1}\sum_{i=1}^{k+1} i\gamma_i \delta_{k+1-i}, \ \ k = 0, 1, 2, \cdots \tag{A5}$$

with $\delta_0 = 1$. It is noted that the same analytical steps have been followed for approximating the aggregate interference term of the sensing function.

Appendix B

In this appendix, a simplified expression for the CDF of s_{max} is presented. Assuming independent and identically distributed shadowing conditions, i.e., $\alpha_j = \alpha$ and $\bar{\gamma}_j = \bar{\gamma}$, and based on probability laws, the CDF of s_{max} is given by

$$F_{s_{max}}(y) = [F_s(y)]^M = \left[\frac{\Gamma(\alpha, \frac{\bar{\gamma}}{y})}{\Gamma(\alpha)}\right]^M. \tag{A6}$$

Assuming integer values for the shaping parameter α and using ([16] [eq. (8.352/2)]), (A6) can be written as

$$F_{s_{max}}(y) = \exp\left(-\frac{\bar{\gamma}M}{y}\right)\left[\sum_{i=0}^{\alpha-1}\left(\frac{\bar{\gamma}}{y}\right)^i \frac{1}{i!}\right]^M. \tag{A7}$$

Finally, using the multinomial identity ([26] [eq. (24.1.2)]), and after some mathematical simplifications, yields

$$F_{s_{max}}(y) = \exp\left(-\frac{\bar{\gamma}M}{y}\right)\sum_{n_1=0}^{M}\sum_{n_2=0}^{M}\cdots\sum_{\substack{n_\alpha=0 \\ n_1+n_2+\cdots+n_\alpha=M}}^{M}\frac{M!}{n_1!n_2!\cdots n_\alpha!}\left[\prod_{i=0}^{\alpha-1}\left(\frac{1}{i!}\right)^{n_{i+1}}\right]\left(\frac{\bar{\gamma}}{y}\right)^{\sum_{i=0}^{\alpha-1}in_{i+1}}. \tag{A8}$$

References

1.	Wild, T.; Braun, V.; Viswanathan, H. Joint design of communication and sensing for beyond 5G and 6G systems. *IEEE Access* **2021**, *9*, 30845–30857. [CrossRef]
2.	Xiao, Z.; Zeng, Y. Waveform Design and Performance Analysis for Full-Duplex Integrated Sensing and Communication. *IEEE J. Sel. Areas Commun.* **2022**, *40*, 1823–1837. [CrossRef]
3.	Liu, M.; Yang, M.; Li, H.; Zeng, K.; Zhang, Z.; Nallanathan, A.; Wang, G.; Hanzo, L. Performance analysis and power allocation for cooperative ISAC networks. *IEEE Internet Things J.* **2022**, *10*, 6336–6351. [CrossRef]
4.	Liu, M.; Yang, M.; Zhang, Z.; Li, H.; Liu, F.; Nallanathan, A.; Hanzo, L. Sensing-Communication Coexistence vs. Integration. *IEEE Trans. Veh. Technol.* **2023**, *72*, 8158–8163. [CrossRef]
5.	Li, X.; Guo, S.; Li, T.; Zou, X.; Li, D. On the Performance Trade-Off of Distributed Integrated Sensing and Communication Networks. *IEEE Wirel. Commun. Lett.* **2023**, *12*, 2033–2037. [CrossRef]
6.	Meng, K.; Masouros, C.; Chen, G.; Liu, F. BS Coordination Optimization in Integrated Sensing and Communication: A Stochastic Geometric View. *arXiv* **2024**, arXiv:2401.04918.
7.	Wu, Q.; Xu, J.; Zeng, Y.; Ng, D.W.K.; Al-Dhahir, N.; Schober, R.; Swindlehurst, A.L. A comprehensive overview on 5G-and-beyond networks with UAVs: From communications to sensing and intelligence. *IEEE J. Sel. Areas Commun.* **2021**, *39*, 2912–2945. [CrossRef]
8.	Zhang, Y.; Shan, H.; Chen, H.; Mi, D.; Shi, Z. Perceptive mobile networks for unmanned aerial vehicle surveillance: From the perspective of cooperative sensing. *IEEE Veh. Technol. Mag.* **2024**, *19*, 60–69. [CrossRef]
9.	Chen, X.; Feng, Z.; Wei, Z.; Gao, F.; Yuan, X. Performance of joint sensing-communication cooperative sensing UAV network. *IEEE Trans. Veh. Technol.* **2020**, *69*, 15545–15556. [CrossRef]
10.	Tropkina, I.; Sun, B.; Moltchanov, D.; Pyattaev, A.; Tan, B.; Dinis, R.; Andreev, S. Distributed communication and sensing system co-design for improved UAV network resilience. *IEEE Trans. Veh. Technol.* **2022**, *72*, 924–939. [CrossRef]
11.	Fei, Z.; Wang, X.; Wu, N.; Huang, J.; Zhang, J.A. Air-ground integrated sensing and communications: Opportunities and challenges. *IEEE Commun. Mag.* **2023**, *61*, 55–61. [CrossRef]
12.	Mei, M.; Yao, M.; Yang, Q.; Wang, J.; Jing, Z.; Quek, T.Q. Network-layer Delay Provisioning for Integrated Sensing and Communication UAV Networks under Transient Antenna Misalignment. *IEEE Trans. Wirel. Commun.* **2024**, *23*, 12964–12979. [CrossRef]
13.	Zhang, C.; Yi, W.; Liu, Y.; Hanzo, L. Semi-integrated-sensing-and-communication (semi-ISaC): From OMA to NOMA. *IEEE Trans. Commun.* **2023**, *71*, 1878–1893. [CrossRef]
14.	Bithas, P.S.; Nikolaidis, V.; Kanatas, A.G.; Karagiannidis, G.K. UAV-to-Ground communications: Channel modeling and UAV selection. *IEEE Trans. Commun.* **2020**, *68*, 5135–5144. [CrossRef]
15.	Simon, M.K.; Alouini, M.S. *Digital Communication over Fading Channels*, 2nd ed.; Wiley: New York, NY, USA, 2005.
16.	Gradshteyn, I.S.; Ryzhik, I.M. *Table of Integrals, Series, and Products*, 6th ed.; Academic Press: New York, NY, USA, 2000.
17.	Al-Hourani, A.; Kandeepan, S.; Lardner, S. Optimal LAP altitude for maximum coverage. *IEEE Wireless Commun. Lett.* **2014**, *3*, 569–572. [CrossRef]
18.	Ren, P.; Munari, A.; Petrova, M. Performance tradeoffs of joint radar-communication networks. *IEEE Wirel. Commun. Lett.* **2018**, *8*, 165–168. [CrossRef]
19.	Fang, Z.; Wei, Z.; Chen, X.; Wu, H.; Feng, Z. Stochastic geometry for automotive radar interference with RCS characteristics. *IEEE Wirel. Commun. Lett.* **2020**, *9*, 1817–1820. [CrossRef]
20.	Bithas, P.S.; Kanatas, A.G.; Matolak, D.W. Exploiting shadowing stationarity for antenna selection in V2V communications. *IEEE Trans. Veh. Technol.* **2018**, *68*, 1607–1615. [CrossRef]
21.	Meng, K.; Masouros, C. Networked ISAC Coordinated Beamforming and Cooperative BS Cluster Optimization. In Proceedings of the 2024 14th International Symposium on Communication Systems, Networks and Digital Signal Processing (CSNDSP), Rome, Italy, 17–19 July 2024; pp. 415–420. [CrossRef]
22.	Adamchik, V.S.; Marichev, O.I. The algorithm for calculating integrals of hypergeometric type functions and its realization in REDUCE system. In Proceedings of the International Symposium on Symbolic and Algebraic Computation, Tokyo, Japan, 20–24 August 1990; pp. 212–224.
23.	Li, X.; Feng, G.; Sun, Y.; Qin, S.; Liu, Y. A Unified Framework for Joint Sensing and Communication in Resource Constrained Mobile Edge Networks. *IEEE Trans. Mob. Comput.* **2023**, *22*, 5643–5656. [CrossRef]
24.	Bithas, P.S.; Ropokis, G.A.; Karagiannidis, G.K.; Nistazakis, H.E. UAV-Assisted Communications With RIS: A Shadowing-Based Stochastic Analysis. *IEEE Trans. Veh. Technol.* **2024**, *73*, 10000–10010. [CrossRef]
25.	Moschopoulos, P.G. The distribution of the sum of independent gamma random variables. *Ann. Inst. Stat. Math.* **1985**, *37*, 541–544. [CrossRef]
26.	Abramowitz, M.; Stegun, I.A. *Handbook of Mathematical Functions: With Formulas, Graphs, and Mathematical Tables*; Courier Corporation: North Chelmsford, MA, USA, 1964; Volume 55.